Supplementary information

Comment on "Two-dimensional honeycomb borophene oxide: strong anisotropy and nodal loop transformation"by C. Zhong, W. Wu, J. He, G. Ding, Y. Liu, D. Li, S. A. Yang and G. Zhang, *Nanoscale*, 2019, 11, 2468-2475

Farid Mohammadi,[a] Kavoos Mirabbaszadeh,*[a] Houshyar Noshad,[a] and Ziba Torkashvand[a]

[a] Department of Energy Engineering and Physics, Amirkabir University of Technology (Tehran Polytechnic), P.O. Box: 159163-4311, Tehran, Iran.

1 Tight Binding Hamiltonian

In this section, our theoretical calculations commence with the evaluation of a h-B_2O tight-binding (TB) Hamiltonian. Within the realm of condensed matter physics, the reciprocal-space Hamiltonian formulation is crucially influenced by two key factors: The first factor pertains to the geometric structure in real space, while the second factor relates to the atomic orbitals. These factors collectively contribute to the comprehensive description of the electronic properties under investigation. Consequently, we begin our analysis by examining the geometric configuration of h-B_2O, where it is evident that the monolayer exhibits a fully planar structure, comprising honeycomb lattices that are stretched along the x-axis. The h-B_2O monolayer demonstrates crystallization in the orthorhombic lattice, characterized by the space group Cmmm (No. 65), furthermore, this structure demonstrates a C_{2v} symmetry. unit cell, is composed of two B and one O atoms (1a). The First Brillouin Zone (FBZ) associated with the structure is represented as a distorted hexagonal shape (due to $\pi/2$ rotation of the unit cell) (1b). The optimum values for the lattice constants, a and b, are 2.806 Å and 7.127 Å, respectively. The lengths of the equilibrium bonds B-B and B-O are 1.706 Å and 1.341 Å, respectively. Due to the presence of the oxygen atom, we have a deformed hexagonal structure whose bond angles are 107.8° and 126.1° respectively [1]. It is time to elucidate the atomic orbitals of h-B_2O. By considering the atomic numbers of boron ($1s^2 2s^2 2p^1$) and oxygen ($1s^2 2s^2 2p^4$), it can be determined that h-B_2O exhibits four orbitals, namely s, p_x, p_y, and p_z. These orbitals determine the electronic properties of h-B_2O. Within this particular framework, we direct our attention toward the orbitals whose energy bands are close proximity to the Fermi level, as they assume a pivotal function in determining the electronic characteristics. Hence, our specific emphasis is directed toward two orbitals, namely p_y, and p_z [2]. But, when considering graphene and β_{12}-

*Email: mirabbas@aut.ac.ir

borophene, it is observed that the p_z orbitals play a prominent role in the conduction process, resulting in the Hamiltonian being exclusively formulated based on these orbitals[3, 4].

Following the elucidation provided regarding the geometric arrangement and the influential orbitals in the electronic characteristics, a TB model is employed to accurately depict the low-energy band structure of h-B_2O. Despite the presence of two B atoms and one O atom in the primitive cell, it is possible to simplify the model by removing the O sites. Since the oxygen atoms occupy a bridging position within the structure, This simplification does not compromise the symmetry of the model [2]. Therefore, to construct a final version of the TB model, we shall take into account the contributions of the p_y and p_z orbitals that are associated with B atoms within the unit cell (see Fig. 2). In order to derive the TB Hamiltonian in the second quantization representation, we analyze each orbital individually. let us begin by examining the p_z orbitals.

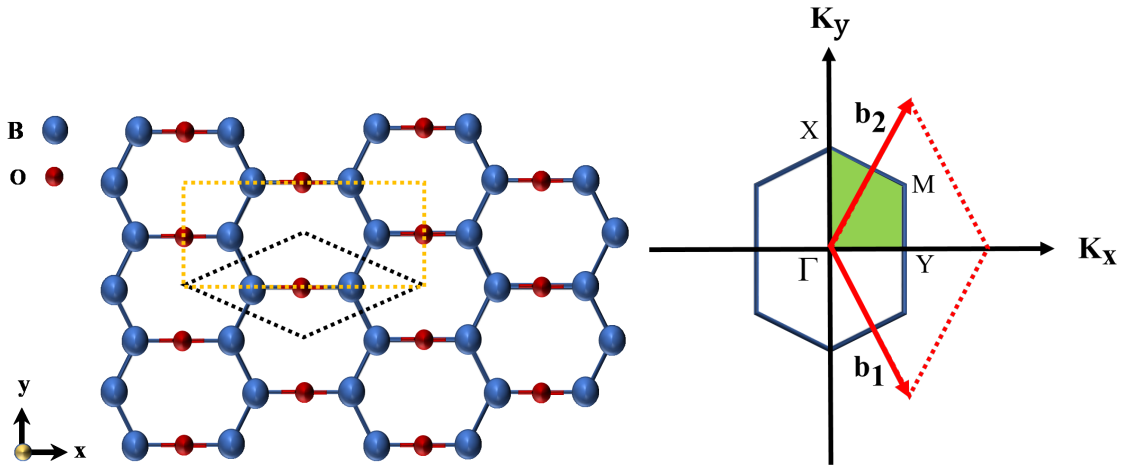

(a) (b)

Figure 1: (a) The crystal structure of h-B_2O. The unit cell is indicated by the yellow dashed line, and the black dashed line marks the rhombic primitive cell. (b) FBZ of h-B_2O

Initially, in relation to the designated atoms within the h-B_2O structure, we shall allocate distinct positions to facilitate the identification of atom hoppings i.e.

$$a \Rightarrow i, \qquad b \Rightarrow j$$

To facilitate comprehension, we initially partition the Hamiltonian into two distinct components:

$$\mathscr{H}_{p_z}^{\vec{k}} = \underbrace{\mathscr{H}_0}_{\text{On-site energies}} + \underbrace{\mathscr{H}_1}_{\text{Hopping energies}} \tag{1}$$

the first section calculates on-site energies, while the second part displays the different hoppings to the nearest-neighbors $\langle NN \rangle$. So,

$$\mathscr{H}_0 = \underbrace{\sum_i \varepsilon_a a_i^\dagger a_i}_{\text{a atom}} + \underbrace{\sum_j \varepsilon_b b_j^\dagger b_j}_{\text{b atom}} \tag{2}$$

$$\mathscr{H}_1 = \underbrace{\sum_{<ij>} t_{ab} a_i^\dagger b_j}_{b \longmapsto a} + \underbrace{\sum_{<ij>} t_{ba} b_j^\dagger a_i}_{a \longmapsto b} \tag{3}$$

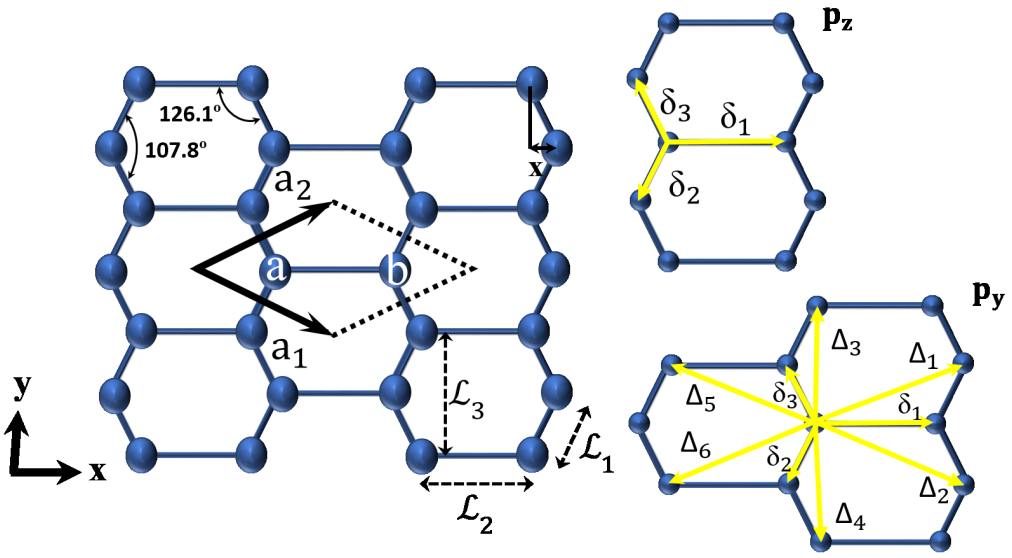

Figure 2: The crystal structure without O atoms, showing the p_y and p_z orbitals of the boron atoms and their respective neighboring atoms.

Two on-site energies for various atoms in the unit cell (ε_a and ε_b) are contained in $\mathscr{H}_0$, and the hoppings from the a atom to the nearest b atoms and vice versa are displayed in $\mathscr{H}_1$. The creation and annihilation operators are denoted as $\{a_i, b_i\}$ and $\{a_i^\dagger, b_i^\dagger\}$, respectively. The final matrix form will be as follows:

$$\mathscr{H}_{p_z}^{\vec{k}} = \begin{bmatrix} \varepsilon_a a_i^\dagger a_i & t_{ij} a_i^\dagger b_j \\ t_{ji} b_j^\dagger a_i & \varepsilon_b b_j^\dagger b_j \end{bmatrix} \tag{4}$$

The coefficient ε_a and ε_b represents the on-site energy of electrons.Since the atoms are the same, ε_a=ε_b. Now, the calculation of creation and annihilation operators is necessary. The relationship between these operators in both real space and reciprocal space can be described as follows:

$$\begin{aligned} a_i &= \frac{1}{\sqrt{N}} \sum_k a_k e^{i\vec{k}.\vec{R}_i} \\ a_i^\dagger &= \frac{1}{\sqrt{N}} \sum_k a_k^\dagger e^{-i\vec{k}.\vec{R}_i} \\ b_j &= \frac{1}{\sqrt{N}} \sum_k b_k e^{i\vec{k}.\vec{R}_j} \\ b_j^\dagger &= \frac{1}{\sqrt{N}} \sum_k b_k^\dagger e^{-i\vec{k}.\vec{R}_j} \end{aligned} \tag{5}$$

where N is the number of unit cells in our system. Hence, we use 5 to calculate $a_i^\dagger b_j$:

$$\begin{aligned} \sum_{\langle i,j \rangle} a_i^\dagger b_j &= \left[\frac{1}{\sqrt{N}} \sum_k a_k^\dagger e^{-i\vec{k}.\vec{R}_i} \right] . \left[\frac{1}{\sqrt{N}} \sum_{k'} b_{k'} e^{i\vec{k'}.\vec{R}_j} \right] \\ &= \sum_{\langle i,j \rangle} \sum_k \sum_{k'} \frac{1}{N} (e^{-i\vec{k}.\vec{R}_i} . e^{i\vec{k'}.\vec{R}_j}) a_k^\dagger b_{k'} \end{aligned} \tag{6}$$

By multiplying $e^{i\vec{k'}.\vec{R}_i}.e^{-i\vec{k'}.\vec{R}_i}$ in 6, we will obtain:

$$\begin{aligned}\sum_{\langle i,j\rangle} a_i^\dagger b_j &= \sum_{\langle i,j\rangle}\sum_k\sum_{k'}\frac{1}{N}(e^{-i\vec{k}.\vec{R}_i}.e^{i\vec{k'}.\vec{R}_i})(e^{-i\vec{k}.\vec{R}_i}.e^{i\vec{k'}.\vec{R}_j})a_k^\dagger b_{k'} \\ &= \sum_k\left[\frac{1}{N}\sum_{k'}e^{i(\vec{k'}-\vec{k}).\vec{R}_i}\right].\left[\sum_{\langle i,j\rangle}e^{i(\vec{R}_j-\vec{R}_i).\vec{k'}}\right]a_k^\dagger b_{k'} \\ &= \sum_k\sum_{\vec{\delta}_{NN}}e^{i(\vec{\delta}_{NN}.\vec{k})}a_k^\dagger b_k = \sum_k f_{\vec{k}}a_k^\dagger b_k\end{aligned} \tag{7}$$

where $\vec{\delta}_{NN} = \vec{R}_j - \vec{R}_i$ is lattice vector and

$$f_{\vec{k}} = \sum_{\vec{\delta}_{NN}} e^{i(\vec{k}.\vec{\delta}_{NN})}$$

In a similar vein, upon substituting the values of variables $b_j^\dagger$ and a_i into the second component of 3 , we obtain:

$$\begin{aligned}\sum_{\langle i,j\rangle} a_i b_j^\dagger &= \sum_k\left[\frac{1}{N}\sum_{k'}e^{i(\vec{k'}-\vec{k}).\vec{R}_j}\right].\left[\sum_{\langle i,j\rangle}e^{i(\vec{R}_i-\vec{R}_j).\vec{k'}}\right]b_k^\dagger a_{k'} \\ &= \sum_k\sum_{\vec{\delta}_{NN}}e^{-i(\vec{\delta}_{NN}.\vec{k})}b_k^\dagger a_k = \sum_k f_{\vec{k}}^* b_k^\dagger a_k\end{aligned} \tag{8}$$

where

$$f_{\vec{k}}^* = \sum_{\vec{\delta}_{NN}} e^{-i(\vec{\delta}_{NN}.\vec{k})} \tag{9}$$

It is now appropriate to present the coordinates of the $\langle NN\rangle$ (all units are in Å):

$$\mathcal{L}_1 = 1.706 = \underbrace{(B-B)}_{\text{bond length}}$$

$$\mathcal{L}_2 = 2.682 = 2\underbrace{(B-O)}_{\text{bond length}}$$

$$x = \sqrt{\mathcal{L}_1^2 - (\mathcal{L}_3/2)^2} = 0.970$$

$$\vec{a}_1 = (\alpha, -\mathcal{L}_3/2) = (3.652, -1.403)$$

$$\vec{a}_2 = (\alpha, \mathcal{L}_3/2) = (3.652, 1.403)$$

$\vec{a}_1$ and $\vec{a}_2$ are the constitutive vectors of the unit cell in real space. where $\alpha = x + \mathcal{L}_2$. Finally, for hopping a to b:

$$
\begin{aligned}
t_1 \rightarrow\ & \{\vec{\delta}_1 = (\mathcal{L}_2, 0) = (2.682, 0) \\
t_2 \rightarrow\ & \begin{cases} \vec{\delta}_2 = (-x, -\mathcal{L}_3/2) = (-0.970, -1.403) \\ \vec{\delta}_3 = (-x, +\mathcal{L}_3/2) = (-0.970, 1.403) \end{cases}
\end{aligned} \tag{10}
$$

and b to a:

$$
\begin{aligned}
\vec{\delta'}_1 &= (\mathcal{L}_2, 0) = (-2.682, 0) \\
\vec{\delta'}_2 &= (x, -\mathcal{L}_3/2) = (0.970, -1.403) \\
\vec{\delta'}_3 &= (x, +\mathcal{L}_3/2) = (0.970, 1.403)
\end{aligned} \tag{11}
$$

Based on condition $a_i b_j = 2\pi\delta_{ij}$ (δ_{ij} is kronecker delta), it is possible to derive the constitutive vectors of the FBZ in the reciprocal lattice.

$$
\begin{aligned}
\vec{b}_1 &= \pi(1/\alpha, -2/\mathcal{L}_3) \\
\vec{b}_2 &= \pi(1/\alpha, 2/\mathcal{L}_3)
\end{aligned} \tag{12}
$$

Finally, the Hamiltonian for the p_z orbital will be as follows, and we will use it in current work to calculate the band structure (BS) and density of states (DOS), as well as to validate our results against density functional theory (DFT) calculations:

$$
\mathscr{H}_{p_z}^{\vec{k}} = \begin{bmatrix} \varepsilon_a & f_{\vec{k}} \\ f_{\vec{k}}^* & \varepsilon_b \end{bmatrix} \tag{13}
$$

where the $f_{\vec{k}}$ is defined as:

$$
f_{\vec{k}} = t_1 e^{ik_x(\mathcal{L}_2)} + [t_2 e^{-ik_x(x)} \cos(k_y(\mathcal{L}_3/2))] \tag{14}
$$

Now, we aim to compute the Hamiltonian for p_y orbitals using the same procedure. So,

$$
\mathscr{H}_{p_y}^{\vec{k}} = \underbrace{\mathscr{H}_0}_{\text{On-site energies}} + \underbrace{\mathscr{H}_1}_{\text{Hopping energies}} \tag{15}
$$

the first section relate to on-site energies of p_y orbitals, while the second part displays the different hoppings to the $\langle NN \rangle$ and next-nearest-neighbors ($\langle NNN \rangle$). As we mentioned, there is one important difference with the p_z orbitals that we must consider: the next-nearest-neighbor interactions for p_y orbitals. Because the p_y orbital lies in the plane of B_2O, considering interactions with $\langle NNN \rangle$ becomes indispensable and should not be disregarded. Therefore, for p_y orbitals, there are three $\langle NN \rangle$ ($\vec{\delta}_1$, $\vec{\delta}_2$, and $\vec{\delta}_3$), sharing the same coordinates as those obtained for the p_z orbitals. Additionally, there are six $\langle NNN \rangle$ ($\Delta_1, ..., \Delta_6$) (see Fig. 2). resulting,

$$
\begin{aligned}
t_1 \rightarrow & \{\vec{\delta}_1 = (\mathcal{L}_2, 0) \\
t_2 \rightarrow & \begin{cases} \vec{\delta}_2 = (-x, -\mathcal{L}_3/2) \\ \vec{\delta}_3 = (-x, +\mathcal{L}_3/2) \end{cases} \\
t_3 \rightarrow & \begin{cases} \vec{\Delta}_3 = (0, +\mathcal{L}_3) \\ \vec{\Delta}_4 = (0, -\mathcal{L}_3) \end{cases} \\
t_4 \rightarrow & \begin{cases} \vec{\Delta}_1 = (\alpha, +\mathcal{L}_3/2) \\ \vec{\Delta}_2 = (\alpha, -\mathcal{L}_3/2) \\ \vec{\Delta}_5 = (-\alpha, +\mathcal{L}_3/2) \\ \vec{\Delta}_6 = (-\alpha, -\mathcal{L}_3/2) \end{cases}
\end{aligned}
\tag{16}
$$

in graphene, which has a regular hexagonal structure with equal bond distances, all bonds share a common hopping parameter [5]. However, in h-B_2O, the presence of oxygen at the bridge site causes the hexagon to deform, resulting in different hopping parameters. Finally:

$$
\mathscr{H}_{p_y}^{\vec{k}} = \begin{bmatrix} \varepsilon_a & g_{\vec{k}} \\ g_{\vec{k}}^* & \varepsilon_b \end{bmatrix} \tag{17}
$$

where $g_{\vec{k}}$ is defined as:

$$
\begin{aligned}
g_{\vec{k}} = & \, t_1 e^{ik_x(\mathcal{L}_2)} + [t_2 e^{-ik_x(x)} \cos(k_y(\mathcal{L}_3/2))] \\
& + 2t_3 \cos(\mathcal{L}_3 k_y) + 4t_4 \cos(k_y(\mathcal{L}_3/2)) \cos(\alpha k_x)
\end{aligned}
\tag{18}
$$

it is worth noting that, due to the orthogonality of the p_y and p_z orbitals, they are found to be independent and decoupled in the TB formalism.

2 BS

To enhance clarity and provide deeper insight, we have depicted the three-dimensional (3D) BS and its corresponding contour plot in Fig. 3a, 3b.

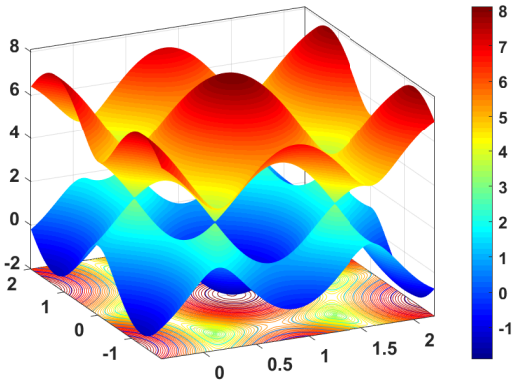

(a)

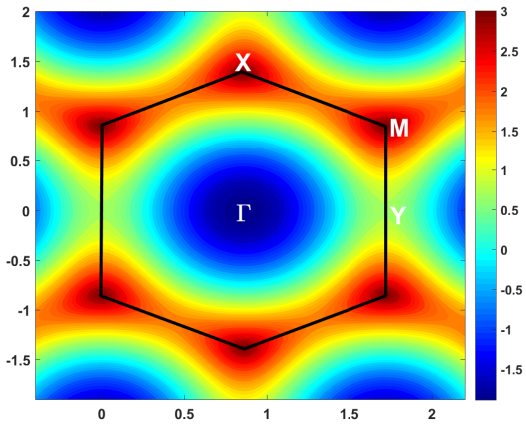

(b)

Figure 3: (a) 3D BS and (b) contour plot of h-B_2O

3 DOS

To determine the DOS for a given system, let us examine a system characterized by a Hamiltonian labeled as $\mathscr{H}$. Here, $\mathscr{E}_n$ and ψ_n represent its normalized eigenvalues and eigenfunctions, respectively. Resulting

$$\mathscr{D}(\mathscr{E}) = \sum_n \delta(\mathscr{E} - \mathscr{E}_n) \tag{19}$$

where $\delta(\mathscr{E} - \mathscr{E}_n)$ represents the Dirac delta function. In the same manner, the Projected Density of States (PDOS) pertaining to orbital Γ_υ within the corresponding system is established as follows.

$$\mathscr{D}_\upsilon(\mathscr{E}) = \sum_n |\langle \Gamma_\upsilon | \psi_n \rangle|^2 \delta(\mathscr{E} - \mathscr{E}_n) \tag{20}$$

where $|\langle \Gamma_\upsilon | \psi_n \rangle|^2$ is the probability of electron presence within orbital Γ_υ. Evidently, the DOS emerges as the aggregate of all PDOS values. This straightforward summation encapsulates the entirety of electronic states distributed across various orbitals, offering a fundamental depiction of the electron density distribution of system.

$$\begin{aligned}\mathscr{D}(\mathscr{E}) &= \sum_{v} D_v(\mathscr{E}) = \sum_{v}\sum_{n} |\langle \Gamma_v|\psi_n\rangle|^2 \delta(\mathscr{E}-\mathscr{E}_n) \\ &= \sum_{n} \delta(\mathscr{E}-\mathscr{E}_n) \underbrace{\sum_{v} |\langle \Gamma_v|\psi_n\rangle|^2}_{=1} = \sum_{n} \delta(\mathscr{E}-\mathscr{E}_n)\end{aligned} \tag{21}$$

it is important to highlight that in the present paper, we have employed PDOS calculations specifically for the p_z and p_y orbitals.

Our goal is to establish the interconnectedness between PDOS and the diagonal components of Green's function. To achieve this, we direct our attention towards an arbitrary element, aiming to elucidate the underlying relationship comprehensively.

$$\begin{aligned}G_{vv}(\mathscr{E}) &= \left\langle \Gamma_v \left| \frac{1}{\mathscr{E}-\mathscr{H}} \right| \Gamma_v \right\rangle \\ &= \sum_{n} \langle \Gamma_v|\psi_n\rangle \left\langle \psi_n \left| \frac{1}{\mathscr{E}+i\eta-\mathscr{H}} \right| \Gamma_v \right\rangle \\ &= \sum_{n} \langle \Gamma_v|\psi_n\rangle \left\langle \Gamma_v \left| \frac{1}{\mathscr{E}-i\eta-\mathscr{H}} \right| \psi_n \right\rangle^* \\ &= \sum_{n} \langle \Gamma_v|\psi_n\rangle \langle \Gamma_v|\psi_n\rangle^* \left(\frac{1}{\mathscr{E}-i\eta-\mathscr{E}_n} \right)^* \\ &= \sum_{n} |\langle \Gamma_v|\psi_n\rangle|^2 \left(\frac{1}{\mathscr{E}-\mathscr{E}_n+i\eta} \right) \\ &= \sum_{n} |\langle \Gamma_v|\psi_n\rangle|^2 \left(\frac{\mathscr{E}-\mathscr{E}_n-i\eta}{(\mathscr{E}-\mathscr{E}_n)^2+\eta^2} \right)\end{aligned} \tag{22}$$

where $\eta = 5$ meV represents the broadening factor. We are now in a position to establish a meaningful link between Dirac delta function definition and the imaginary component of equation22. This connection propels us toward our main aim, which involves the calculation of DOS.

$$\delta(x) = \lim_{a\longrightarrow 0} \frac{1}{\pi} \frac{a}{x^2+a^2} \tag{23}$$

Consequently

$$\begin{aligned}\lim_{\eta\longrightarrow 0} ImG_{vv}(\mathscr{E}) &= \lim_{\eta\longrightarrow 0} \sum_{n} \langle \Gamma_v|\psi_n\rangle|^2 \left(\frac{-\eta}{(\mathscr{E}-\mathscr{E}_n)^2+\eta^2} \right) \\ &= -\pi \sum_{n} |\langle \Gamma_v|\psi_n\rangle|^2 \delta(\mathscr{E}-\mathscr{E}_n)\end{aligned} \tag{24}$$

finally for PDOS and DOS:

$$\begin{aligned}\mathscr{D}_v(\mathscr{E}) &= \sum_{n} |\langle \Gamma_v|\psi_n\rangle|^2 \delta(\mathscr{E}-\mathscr{E}_n) = \frac{1}{\pi} \lim_{\eta\longrightarrow 0} \mathbf{Im} G_{vv}(E) \\ \mathscr{D}(\mathscr{E}) &= \sum_{v} \mathscr{D}_v(\mathscr{E}) \frac{1}{\pi} \lim_{\eta\longrightarrow 0} \mathbf{Im}[\mathbf{Tr} G(\mathscr{E})]\end{aligned} \tag{25}$$

as an illustration, for p_z orbitals in the FBZ, PDOS will be depicted as:

$$\mathscr{D}_{p_z}(\mathscr{E}) = -\frac{1}{\pi N_a} \sum_{\vec{k}\in FBZ} \mathbf{Im}[\mathbf{Tr}G(\vec{k}, \mathscr{E})] \tag{26}$$

where N_a represents the number of atoms per unit cell [6, 7].

4 Comparison of Our BS and DOS Results with Zhong et al.

In this section, we compare our results with those reported by Zhong et al. To begin, we present both BS together, which highlight the key differences between our work and that of Zhong et al., providing clearer insights for readers (see Fig. 4).

Table 1: Optimized parameters, including on-site energies and hopping values for the two orbitals, p_y and p_z, of the boron atom (all values are in eV) in Zhong et. al.'s study.

Orbital	ε_α	t_1	t_2	t_3
P_y	-3.7	1.5	-1.9	0.7
P_z	2.6	1.35	-1.78	-

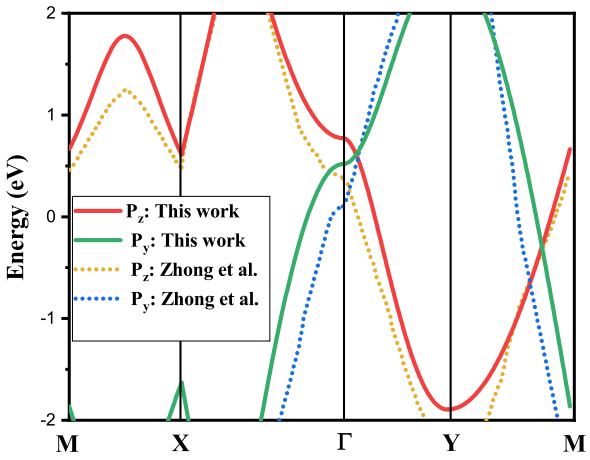

Figure 4: BS of h-B_2O using the TB approximation for the P_y and P_z orbitals: results from this work and those adapted from Zhong et al. [2], with permission from the Royal Society of Chemistry.

We also compare the DOS for the P_y and P_z orbitals (see Fig. 5 and 6). Notably, Zhong et al. did not report a DOS diagram based on TB coefficients in their study. Therefore, using their on-site energies and hopping parameters (see Table. 1), and applying the Green's function approach introduced earlier, we generated the corresponding DOS diagrams. These results demonstrate the superior accuracy of our calculations, as the on-site energies and Van Hove singularities in Zhong et al.'s work appear to be inaccurately reported. For better clarity, we present the DOS diagrams in two different energy ranges: a wider range to clearly show the on-site energies,

and a narrower range (-2 eV to 2 eV) to match the energy window used in the BS plots. We attribute these discrepancies to two main issues discussed in our article: (I) the absence of the HSE approximation, and (II) an oversight in including four next-nearest-neighbor interactions for the P_y orbital - the same orbital that exhibits the greatest inconsistency in their DOS plot.

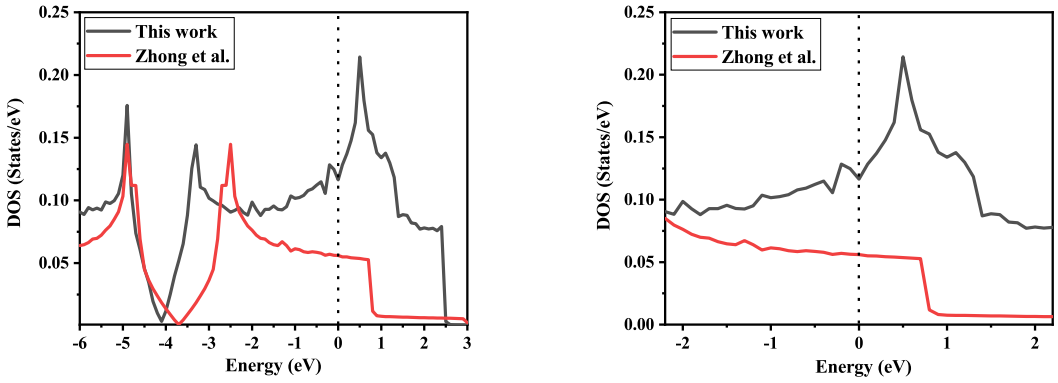

(a) (b)

Figure 5: DOS as a function of energy for the P_y orbital: results from this work (black solid line) and Zhong et al. (red solid line).

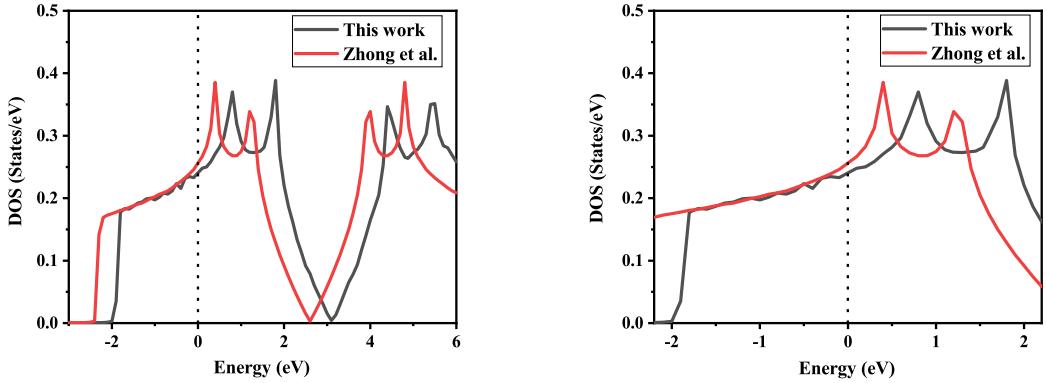

(a) (b)

Figure 6: DOS as a function of energy for the P_z orbital: results from this work (black solid line) and Zhong et al. (red solid line).

References

[1] Luo Yan, Peng-Fei Liu, Hengtao Li, Yong Tang, Junjie He, Xingyong Huang, Bao-Tian Wang, and Liujiang Zhou. Theoretical dissection of superconductivity in two-dimensional honeycomb borophene oxide b2o crystal with a high stability. *npj Computational Materials*, 6(1):94, 2020.

[2] Chengyong Zhong, Weikang Wu, Junjie He, Guangqian Ding, Yi Liu, Dengfeng Li, Shengyuan A Yang, and Gang Zhang. Two-dimensional honeycomb borophene oxide: strong anisotropy and nodal loop transformation. *Nanoscale*, 11(5):2468–2475, 2019.

[3] Jeil Jung and Allan H MacDonald. Tight-binding model for graphene π-bands from maximally localized wannier functions. *Physical Review BCondensed Matter and Materials Physics*, 87(19):195450, 2013.

[4] Motohiko Ezawa. Triplet fermions and dirac fermions in borophene. *Physical Review B*, 96(3):035425, 2017.

[5] Stephanie Reich, Janina Maultzsch, Christian Thomsen, and Pablo Ordejon. Tight-binding description of graphene. *Physical Review B*, 66(3):035412, 2002.

[6] Gerald D Mahan. *Many-particle physics*. Springer Science & Business Media, 2013.

[7] Khang D Pham, Nguyen D Hien, Nguyen N Hieu, and Le TT Phuong. Magnetic properties of β12-borophene in the presence of electric field and dilute charged impurity. *Physica E: Low-dimensional Systems and Nanostructures*, 120:114074, 2020.